DEMONSTRATION OF TUNABLE ENERGY PROPAGATION USING MAGNETO-MECHANICAL OSCILLATOR ARRAYS

Robin E. Carroll[1], Jared A. Little[2], Brian P. Mann[2], and David P. Arnold[1]
[1]University of Florida, Gainesville, FL, USA
[2]Duke University, Durham, NC, USA

ABSTRACT

This work reports, for the first time, a MEMS testbed platform that not only demonstrates complex energy propagation behaviors in periodic arrays of magnetically coupled mechanical oscillators, but also a technique to alter those behaviors externally, after fabrication of the device. Using the microfabricated oscillator arrays, we show frequency bandgaps and a technique to modify the bandgap response, providing valuable experimental data to validate theoretical models. Additionally, the devices demonstrate that those behaviors are affected by the strength of the inter-oscillator coupling force and stiffness of the array oscillators. Each device consists of multiple 1-D arrays of microfabricated magnet-on-cantilever oscillators, utilizing the magnets for inter-oscillator coupling and transmission of energy. Through experimental investigation of these behaviors, fundamental insights can be applied to sensors, shock absorption, filters and energy conversion systems.

INTRODUCTION

When excited by an external force, coupled oscillators arranged in a periodic structure are predicted to respond with a variety of interesting wave propagation behaviors such as frequency bandgaps [1] and energy localizations [2]. Furthermore, recent macro-scale experiments (1-10 Hz range) have shown it is possible to passively switch between bandgap behaviors through the addition of dynamic nonlinearity [3]. The system dynamic behaviors are dependent on the oscillator masses, coupling forces, and individual restoring forces [1,4]. Compared to macroscale dynamic testbeds, MEMS fabrication techniques offer the advantages of batch manufacturing of arrays of large numbers of oscillators with, ideally, identical performances and a wide range of operation frequencies (100's of Hz to 10's of kHz) that can be tuned based on design and post-fabrication parameters.

In order to realize bandgap response behaviors, a periodic array of magnetically coupled oscillators with alternating smaller and larger masses is used, like that shown in the block diagram of Figure 1. Excitation is provided at one end by magnetically actuating the first oscillator in the array via a sinusoid, which stimulates energy propagation down the long axis of the array.

The primary factors that influence bandgap behavior (the frequency range and bandwidth) in an array include the local oscillator stiffness (k), the proof mass (m), the coupling stiffness (k_{mag}), and the unit cell mass ratio. Therefore, variations in those parameters allow for exploration of how they affect the frequency range (cut-on and cut-off frequency values) and width of a bandgap response.

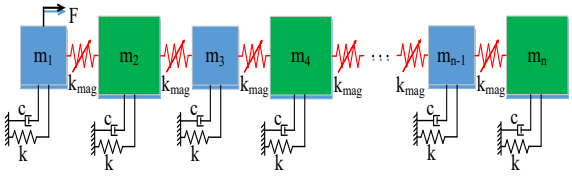

Figure 1: Block diagram of array oscillator dynamics

MAGNETO-MECHANICAL DEVICE

Design

Devices are designed and fabricated using silicon on insulator (SOI) wafers to create arrays of silicon cantilever beams with an incorporated proof mass and micromagnet at the end of the beam (Fig 2). Two types of devices are fabricated, the difference being the magnetic material: either nickel-iron (NiFe), a soft magnetic material (Fig. 2A), or samarium-cobalt (SmCo), a permanent (hard) magnet (Fig. 2B).

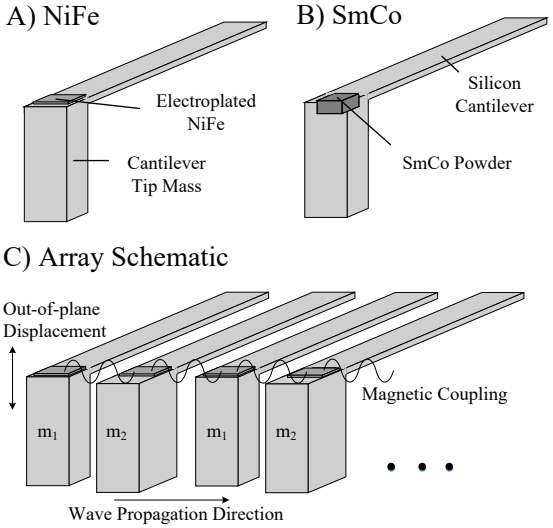

Figure 2: Diagram of single oscillator designs for (A) NiFe and (B) SmCo oscillators and (C) a schematic for array dynamics.

The soft magnets are 15-µm-thick, electroplated NiFe which provide oscillator coupling strength dependent on an externally applied B-field. The hard magnets are SmCo powder embedded/bonded in 50-µm-deep, DRIE-etched trenches, which are pulse-magnetized in-plane [5]. When placed in close enough proximity, the magnets provide a coupling force to allow wave propagation down the array when displaced, as shown in Fig. 2C.

To explore various design parameters, five oscillator unit cell designs are used, summarized in Fig. 3 and Table 1. Designs A, B, D, and E vary the local stiffness via the beam lengths, while design C varies the coupling stiffness via difference in magnet-to-magnet separation compared to design B. All designs use a tip mass ratio of 2:1 to

provide the mass asymmetry in the unit cell, which is required for formation of a bandgap.

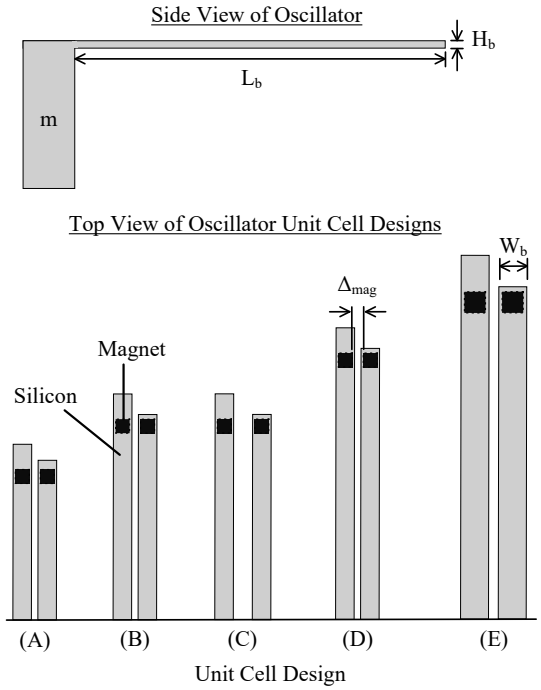

Figure 3: Side view (top) of an oscillator and comparison diagram (bottom) of unit cell designs A – E.

Table 1. Oscillator unit cell designs.

Array Parameter		Array Design Type				
		A	B	C	D	E
Beam length (μm)	L_b	1250	1500	1500	1750	2000
Beam width (μm)	W_b	150	150	150	150	175
Beam height (μm)	H_b	7	7	7	7	7
Mag. spacing (μm)	Δ_{mag}	80	80	110	80	92
Proof mass 1 (μg)	m_1	0.32	0.32	0.32	0.32	0.40
Proof mass 2 (μg)	m_2	0.65	0.65	0.65	0.65	0.81

Bandgap Modeling

With the physical dimensions and materials of the oscillators determined, the key parameters (k, m, k_{mag}) are estimated for each design via analytical means in order to model the predicted bandgap behavior. Note, only the SmCo arrays are considered for modeling purposes, since the k_{mag} parameter of the NiFe versions depend on the strength of an externally applied magnetic field (B-field).

The simplified model used here ignores damping, assumes an infinite array, and solves for the eigenvalues of one unit cell within the system. The equation of motion (EOM) of the n^{th} and $n^{th}+1$ oscillators is found via inspection of a block diagram like that of Fig. 1, e.g.

$$m_n\ddot{x}_n + kx_n + k_{mag}(2x_n - x_{n-1} - x_{n+1}) = 0 \qquad (1)$$

where x represents the displacement of the oscillator indicated by the subscript. Next, a travelling wave solution is assumed of the form of

$$x(\omega, t) = A_n e^{i(j\gamma - \omega t)} \qquad (2)$$

where A_n is amplitude, j is the wave propagation direction which can equal 1 or -1 (1 in this case), γ is the wavenumber, ω is the angular frequency, and t is time. Equation (2) is inserted into (1), creating a system of equations, which is represented in matrix form as

$$[\mathbf{K} - \omega^2 \mathbf{M}]\,\mathbf{A} = 0 \qquad (3)$$

Here, **K** represents the stiffness matrix of the system (including both local and coupling stiffness), **M** the mass matrix, and **A** the amplitude matrix (which can be assumed to be 1 for the purposes of the model). The eigenvalues of (3) are solved for over a range of wavenumber inputs to determine the propagation frequencies for a given system design.

Microfabrication Process

The microfabrication processes for the SmCo and NiFe both begin with a (100) silicon-on-insulator (SOI) wafer with 7 μm device layer, 1 μm buffered oxide (BOX) layer of SiO_2, and a 525 μm handle layer. The SmCo process flow, shown in Figure 4, starts by dry etching the 50 μm deep magnetic powder cavities via first etching using a deep reactive ion etching (DRIE) process for the device layer, a reactive ion etching (RIE) process for the BOX layer, and another DRIE process for the handle layer (Fig. 4B). The SmCo powder is then packed into the cavities (Fig. 4C) and bonded together via physical vapor deposition of parylene C polymer [5], which is then patterned to only cover the oscillator magnets via O_2 plasma (Fig. 4D).

The oscillator cantilever beams are then formed via a 250 μm dry etch using DRIE-RIE-DRIE (Fig. 4E). The wafer is then prepared for the backside etch to form the proof masses of the oscillators by patterning the mass areas on the backside and attaching the wafer to a carrier for the backside DRIE process, which also serves to release the devices (Fig. 4F-4G). The formed devices are then removed from the carrier via a long photoresist strip (Fig. 4H) and then magnetized along the long axis of the arrays using a 7 T pulsed magnetic field.

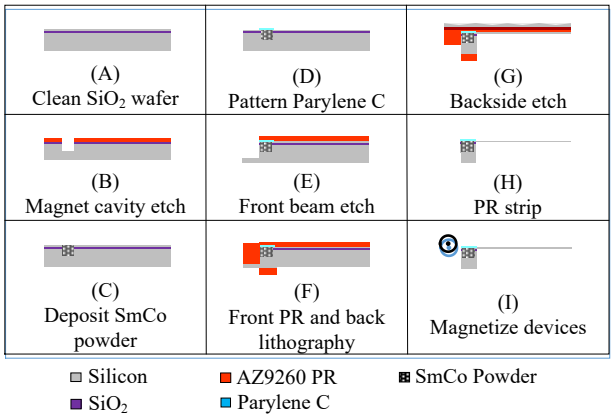

Figure 4: SmCo Device microfabrication steps: (A) – (D), SmCo magnet fabrication; (E)-(F), beam formation; (G) – (I), proof mass formation and device release etch.

For the NiFe array versions, the NiFe magnets use seed layers of Ti (10 nm), Cu (150 nm), and Ti (10 nm) (Fig. 5B) on the SOI. The molds for the magnets are then made from a 21 µm-thick AZ9260 photoresist (PR) (Fig. 5C). The exposed Ti is wet etched with diluted hydrofluoric acid (HF) to expose the Cu layer areas, where 15 µm-thick NiFe is electroplated (Fig. 5D). Once a layer of PR is patterned over the NiFe, the surrounding Ti and Cu seed layers are wet etched. The remainder of the process flow is identical to the SmCo beam and proof mass formation process. Examples of the completed devices are pictured in Fig. 6.

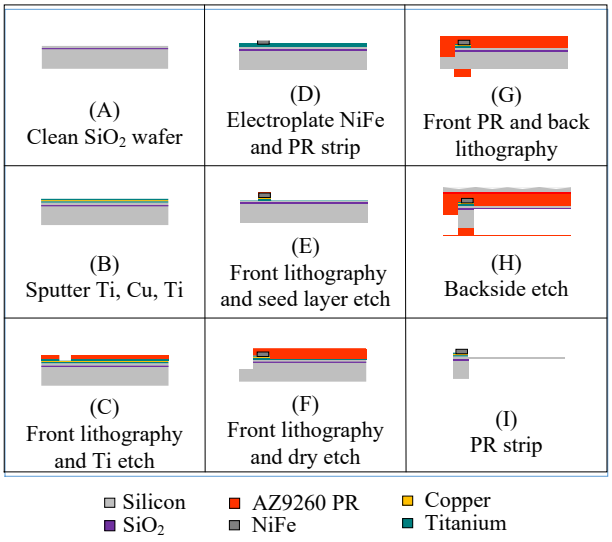

Figure 5: NiFe device microfabrication steps: (A) – (D), NiFe magnet fabrication; (E)-(F), beam formation; (G) – (I), tip mass formation and device release etch.

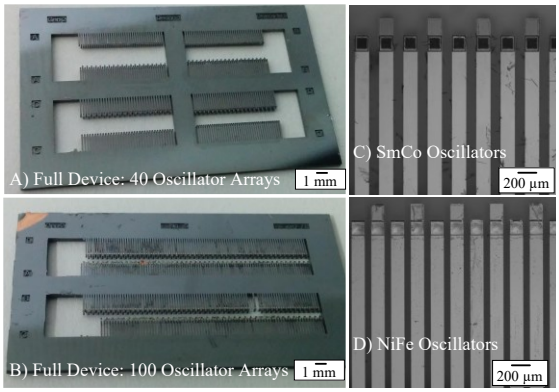

Figure 6: Images of a fabricated (A) full device with 8 separate arrays, (B) full device with 4 separate long arrays, (C) SmCo oscillators, and (D) NiFe oscillators.

EXPERIMENTAL DESIGN

Testing is performed by measuring the out-of-plane displacement of each oscillator in an array while the array is being excited at one end under controlled conditions. During testing, the first oscillator in an array is driven by an excitation magnet attached to a piezo stack actuator (Fig. 7A) receiving a sinusoidal input to maintain a 10 µm pk-to-pk displacement. The actuator and device are mounted to x-y axis and z axis micrometer stages respectively (Fig. 7B). That setup is then mounted under a laser Doppler vibrometer (LDV), which measures the out-of-plane displacement of the oscillators (Fig. 7C). The voltage signal from the LDV system is recorded and subsequently post-processed to determine the frequency and amplitude of the measured oscillator response. Each oscillator in the array is measured individually using a frequency sweep (25 Hz steps), and the results from all oscillators compiled to form the array response.

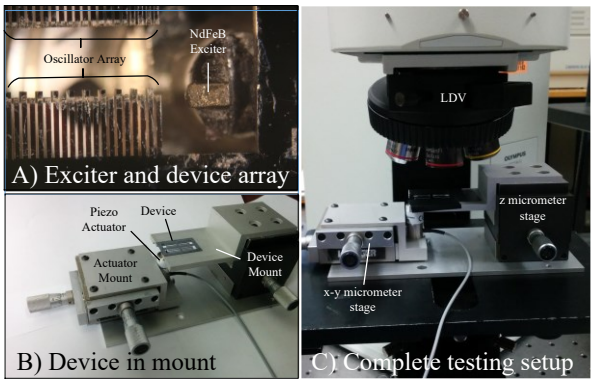

Figure 7: Images of (A) exciter magnet and partial array, (B) Mounted device, and (C) complete setup.

RESULTS

Samarium-Cobalt Devices

An array of each unit cell design (A - E) of the SmCo versions are tested using the procedure outlined in the previous section. The clear separation (in frequency) of two pass bands indicate the presence of a bandgap in the array. To clearly define the edges of the bandgap, a half-power bandwidth method is applied, where the edges of the bandgap (cut-on and cut-off frequencies) are defined where no oscillator in the array exhibits a displacement greater than -3 dB of the maximum measured value.

To analyze the data from a given array, spectrographic plots are made like the example for a SmCo type A array shown in Fig. 8. Here, the oscillator number is plotted on the y axis, with the excitation frequency plotted on the x axis. The bandgap region is highlighted as occurring between 750 Hz and 825 Hz.

The same tests are repeated for SmCo arrays of designs B – E. Fig. 9 summarizes the measured and predicted bandgaps showing the measured frequency ranges fall within the predicted ranges for all five.

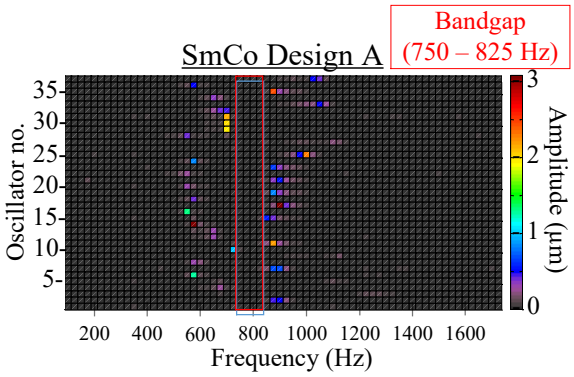

Figure 8: Spectrograph plot of data obtained from SmCo array test showing bandgap between 750 Hz and 825 Hz.

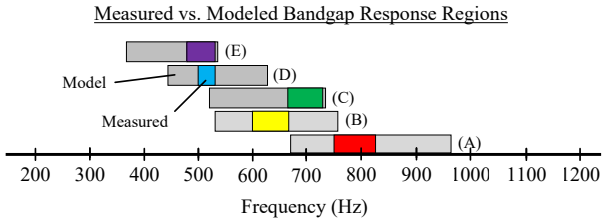

Figure 9: Modeled (gray) vs. measured (color) bandgap responses for SmCo arrays of designs A – E.

Nickel-Iron Devices

The same testing procedure is repeated for a NiFe device of type B while it is within a zero, low, and high magnetic field. The applied B-field source is either zero, one or three - 5/8" dia x 1/8" thick NdFeB magnets arranged relative to the device as shown in the schematic to the right of each data plot in Figure 9. As the B-field strength increases from Fig. 10A to 9C, as does the inter-oscillator coupling stiffness and thus the apparent bandgap response behavior. It is apparent from the plotted results that the bandgap response can be turned off and on using this method and to a lesser extent modified. However, a finer control of the magnetic field is believed to give a finer control of the bandgap response behavior and is a consideration for future work.

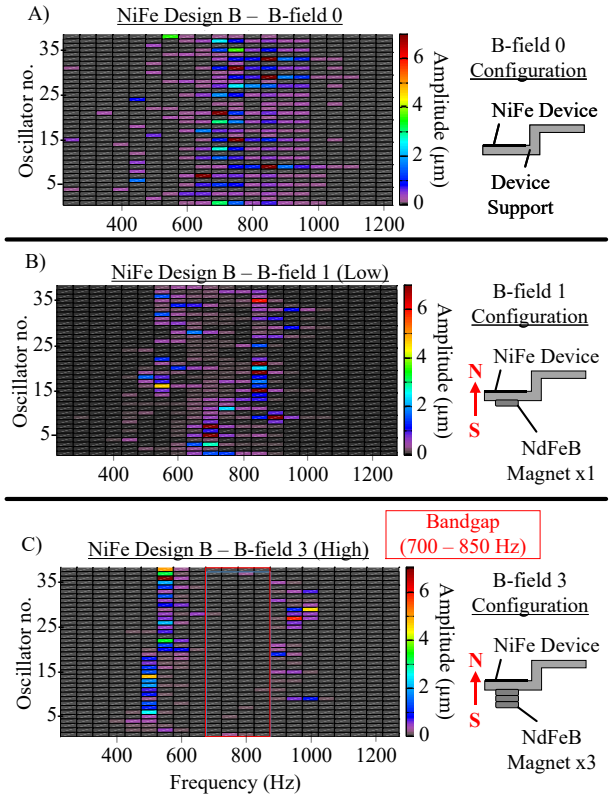

Figure 10: NiFe array test with no applied B-field (A), low B-field (B) and high B-field (C).

CONCLUSION

The accomplishments achieved in this work include the demonstration of a bandgap response in an array of microfabricated oscillators; the ability to characterize the bandgap response behaviors based on design parameters and fit those behaviors to a model; and a technique by which the bandgap response can be modified post-fabrication.

Using both SmCo and NiFe devices, the bandgap behavior is shown and quantified in all tested arrays. The shift in bandgap between the tested SmCo arrays is attributed to the difference in local stiffness of each array design. Similarly, the NiFe array shows a change in the bandgap response, but this is dependent on the external magnetic field applied.

Future work for this research can include bandgap prediction model refinement and improvements to increase the precision of the applied B-field strength. To summarize, these devices demonstrate frequency bandgaps and post-fabrication modification of a bandgap response in a single MEMS based platform.

ACKNOWLEDGEMENTS

This work was supported in part by the U.S National Science Foundation (CMMI-1300658). The authors thank the staff of the UF Nanoscale Research Facility for assistance with the microfabrication.

REFERENCES

[1] M. Sato, et al. "Nonlinear energy localization and its manipulation in micromechanical oscillator arrays," *Rev. Modern Physics*, vol. 78, pp. 137–155 (2006).

[2] J. S. Jensen, "Phononic band gaps and vibrations in one- and two-dimensional mass-spring structures," *J. Sound Vibration*, vol. 266, pp. 1053–1078 (2003).

[3] B. P Bernard, et al. "Experimental investigation of bifurcation induced bandgap reconfiguration", *J. Appl. Phys.*, vol. 116, no. 8, 084904 (2014).

[4] J.A. Little, et al. "Investigation of Wave Propagation Behavior in Magnetically Coupled MEMS Oscillators." *ASME 2015 International Design Engineering Technical Conferences and Computers and Information in Engineering Conference*. American Society of Mechanical Engineers, 2015.

[5] O. D. Oniku, B. J. Bowers, S. B. Shetye, N. Wang, and D. P. Arnold, "Permanent magnet microstructures using dry-pressed magnetic powders," *J. Micromech. Microeng.*, vol. 23, no. 7, 075027, 11 pages (2013)..

CONTACT

*R.E. Carroll, tel: +1-804-5133051; robcarroll@ufl.edu